CONVECTIVELY UNSTABLE WAVE PACKETS IN A FILM FLOW ON AN INCLINED PLANE

L. Brevdo*, T.J. Bridges†, F. Dias° and P. Laure°
* Ecole Supérieure de Mécanique de Marseille, 13451 Marseille cedex 20, France,
° Institut Non-Linéaire de Nice, 1361 route des Lucioles, 06560 Valbonne, France,
† Department of Mathematics and Statistics, Guildford, Surrey, GU2 5XH England, UK

ABSTRACT

The initial-boundary-value linear stability problem for localised disturbances in a film flow on an inclined plane is treated. The linearised Navier-Stokes equations are solved both for localised disturbances having the form of pulses, as well as for perturbations induced by spatially localised periodic in time forcings. Unstable wave packets are analysed by using the formalism of absolute and convective instabilities based on the exact collision criterion [1] for multiple $k-$roots of $D(k,\omega)=0$, where k is a wavenumber, ω is a frequency and D is the dispersion relation function. For a wide range of parameters relevant to experiments [2, 3] the instability is shown to be convective. These results are compared to those obtained by means of the saddle point treatment [4]. This comparison shows a failure of this latter treatment to recover a subinterval of the interval of unstable ray velocities V for large Reynolds number ($R > 100$). This can be observed experimentally because of the abrupt increase by a factor of about 5.3 of the wavelength across the wavepacket associated with the appearance of this branch. This behavior is also found for a falling film. Moreover, properties of spatially amplifying waves were computed for a parameter range relevant for available measurements. The main feature is that the spatial amplification can be deduced very accurately from the temporal stability by applying the Gaster's relation [5]. The computations compare well with experimental data [2].

1 Introduction

Experimental evidence and analysis of model equations show that the absolute and convective dichotomy is important for both the primary and the secondary instabilities observed in viscous film flow. Recent experiments of Liu & Gollub [6, 7] and Liu, Paul & Gollub [2] confirmed the primary neutral stability curve of Benjamin [8] and Yih [9], and several new observations were made as well. In Liu *et al.* [2] strong evidence was presented for convective instability in all cases. In Liu & Gollub [6] unstable periodic waves were tracked until they developed a spatially chaotic structure. For the range of parameters studied, they also found that the secondary instability was strictly convective. Secondary, subharmornic and three dimensional instabilities [6, 10] in thin film are also widely studied because their behaviors are comparable to thoses observed in other shear flows such as boundary layers.

Recent results on model equations for thin-film flow have been reviewed in Chang [11] and Chang & Demekhin [3]. Theoretical aspects of the classification of instabilities as absolute or convective for thin film flow have been addressed in Joo & Davis [12]. In that paper the role of absolute and convective instabilities associated with the primary instability of thin-film flow was studied using a model equation and they found predominantly convective instability; but they also found regions in parameter space where the instability is absolute. The linearised model equation used in the analysis of Lin [13] is absolutely unstable for all parameter values in the unstable range. In Chang & Demekhin [3] the falling film flow was shown to be absolutely stable for all Reynolds numbers below 750 (or 500 for a Reynolds number scaled with the flow rate) by treating the full linearised Navier-Stokes equations.

In this paper we study the initial-value problem for the full Navier-Stokes equations linearised about the basic parabolic velocity profile for thin-film flow analytically, using the Fourier-Laplace transform to reduce the linearised Navier-Stokes equations to an inhomogeneous Orr-Sommerfeld equation coupled to inhomogeneous boundary conditions. The resulting boundary-value problem is treated numerically using a spectral (Chebyshev polynomials) method. Our main results are threefold. First, we give an absolute and convective instability classification of the full problem and describe properties of unstable wave packets for a large and experimentally relevant range of the parameter space. Secondly, we show that absolute instability predicted by the model equations in Joo & Davis [12] and in Lin [13] is anomalous and is not a property of the full equations – indeed, for all values of parameters studied here we find that the primary instability is convective, in agreement with all known experiments. Thirdly, we find that a straightforward application of the saddle point technique even in an apparently accurate way to discriminate between absolute and convective instabilities fails due to an interesting bifurcation that takes place in the complex wavenumber plane. This observation is fundamental and could have wide implications in fluid mechanics where simple saddle-point criteria are applied. As far as we are aware this is the first observation of such a dispersion relation singularity in a fluid mechanics problem.

2 Formulation

We consider a two-dimensional film flow of homogeneous incompressible viscous fluid of viscosity μ and density ρ down an inclined flat plate having an angle θ with the horizontal, see Fig. 1.

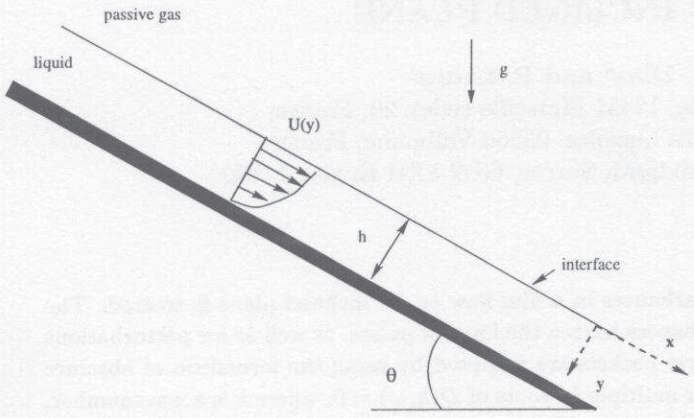

Figure 1: Geometric configuration and coordinate system.

The film thickness in the absence of disturbances is h, the gas above the film is assumed to be passive, the surface tension on the interface between the fluid and the gas is T. The basic unidirectional flow parallel to the plate is driven by the component $g\ \sin\ \theta$ of the gravity along the plate. There is a basic hydrostatic pressure gradient perpendicular to the plate induced by the component $g\ \cos\ \theta$ of gravity normal to the plate. In the coordinate system (Oxy), with x and y being the coordinates parallel and perpendicular to the plate, respectively, and with the origin O on the unperturbed interface, the non-dimensional basic state is given by

$$U(y) = 1 - y^2, \quad P(y) = 2y\ \cot\ \theta, \quad 0 \leq y \leq 1, \qquad (1)$$

where $U(y)$ is the $x-$component of the velocity vector and $P(y)$ is the pressure. All length are made dimensionless with respect to h, speeds with respect to $U_0 = (\rho g h^2\ \sin\ \theta)/2\mu$, and the pressure is scaled by $\mu U_0/h$.

The two-dimensional linear perturbation dynamics of the film flow is governed by the Navier-Stokes equations linearised around the basic state (1) that, in the absence of external sources and perturbations, read

$$\begin{aligned} &Ru_t + R[U(y)u_x + U'(y)v] = -p_x + \nabla^2 u, \\ &Rv_t + RU(y)v_x = -p_y + \nabla^2 v, \\ &u_x + v_y = 0, \\ &(y, x, t) \in (0,1) \times \mathbb{R} \times \mathbb{R}^+. \end{aligned} \qquad (2)$$

Here, u and v are the $x-$ and $y-$components of the perturbation velocity, respectively, p is the perturbation pressure, $R = U_0 h\rho/\mu = \rho^2 g h^3 \sin\ \theta\ /(2\mu^2)$ is the Reynolds number, $\nabla^2 = \partial^2/\partial x^2 + \partial^2/\partial y^2$, and the prime denotes $\mathrm{d}/\mathrm{d}y$. When no disturbances are imposed on the boundaries, (i) the interface $y = \eta(t,x)$ is composed of flow trajectories (the kinematic condition), (ii) the shear stress at the interface is zero, (iii) the normal stress at $y = \eta(t,x)$ is balanced by the surface tension times the curvature (two dynamic conditions), and (iv) the fluid velocity vanishes at the plate $y = 1$ (the non-penetration and non-slip conditions). These conditions linearised around the basic state (1) are

$$\eta_t + U\eta_x - v = 0, \qquad \text{at} \qquad y = 0, \qquad (3)$$

$$u_y + v_x + U''\eta = 0, \qquad \text{at} \qquad y = 0, \qquad (4)$$

$$2v_y - p - P'\eta + 2W\eta_{xx} = 0, \qquad \text{at} \qquad y = 0, \qquad (5)$$

$$u = 0, \quad v = 0, \qquad \text{at} \qquad y = 1. \qquad (6)$$

In (5), $W = \Gamma/(gh^2\ \sin\ \theta)$ is the Weber number, with $\Gamma = T/\rho$.

3 Temporal Linear Stability

Before stuying the convective or absolute nature of instabilities, we make some remarks concerning the temporal stability properties of the flow. That means that we look at wether periodic perturbations in the form $\hat{f}(y)\ \exp[\mathrm{i}(kx - \omega t)]$ are amplified or not (k_r is the wavenumber, $k_i = 0$, ω_i is the growth rate whereas ω_r is the pulsation of the perturbation). Floryan *et al.* [14] have performed theses computations for small angles and found out that, in this case, two unstable modes exist: a shear mode and a surface mode. For very small angles of less than about $0.5'$, a destabilisation of the flow occurs as a result of a shear mode instability. For angles greater than about $0.5'$, a destabilisation is caused by a surface mode instability, and for moderate unstable values of the Reynolds number no unstable shear mode is present. For the surface mode, in the longwave limit $k = k_r \to 0$, one has

$$\omega = 2k_r + i\ \frac{2}{15}(-5\ \cot\ \theta + 4\ R)k_r^2 + o(k_r^2). \qquad (7)$$

Hence, in this limit,

$$R_c = 5\ \cot\ \theta/4 \qquad (8)$$

is the critical Reynolds number. Computations of Floryan *et al.* [14] showed that R_c given in (8) is the critical Reynolds number of the flow when destabilisation is caused by a surface mode instability because such a destabilisation occurs for infinitely long waves. In Fig. 2, computations of the growth rate ω_i as a function of k_r, presented for several values of the Reynolds number, illustrate this destabilisation. The computations are performed by using a pseudo-spectral method to discretize the homogeneous boundary-value problem associated with the problem [15]. The physical parameter values in Fig. 2 are those used in the experiments [2].

From Fig. 2, it is clearly seen that the growth rate ω_i satisfies quantitatively (7) in the unstable case only for very small k_r. Since the size of the interval of the unstable wavenumbers in this figure is of order one, for R as low as 20, the longwave approximation is not suitable for investigating wavepacket asymptotics in this flow.

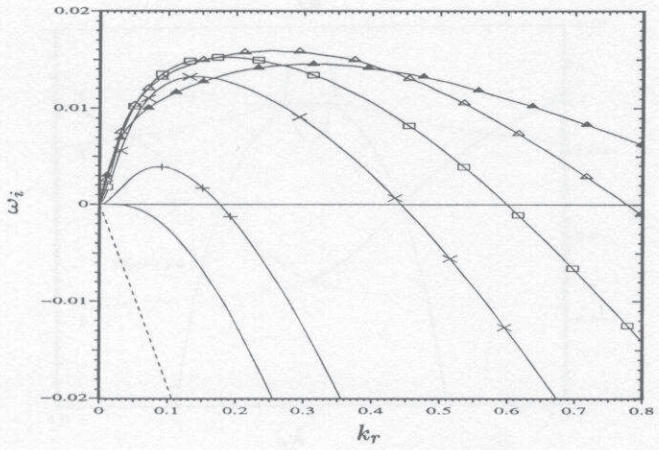

Figure 2 : Growth rate ω_i as a function of k_r for various values of the Reynolds number: $R = 10$ (- -), R_c (–), 20 (+), 40 (×), 60 (□), 100 (△), and 200 (▲). Parameter values: $\theta = 4.6°$, $\nu = 5.02 \times 10^{-6}\mathrm{m}^2/\mathrm{s}$, $T = 69 \times 10^{-3}\mathrm{N/m}$, and $\rho = 1.13\ \mathrm{g/cm}^3$.

4 Absolute and convective instabilities

A laminar flow is called linearly absolutely unstable if small localized perturbation grow in time at the location of excitation. If any unstable localized disturbance propagates away from the location of its origin without affecting the basic state flow, then the flow is called convectively unstable, but absolutely stable [1, 16, 17]. In order to determine the nature of interfacial instabilities, we look a the properties of the propagating unstable wave packets and spatially amplifying waves.

A wave packet approach in the linear stability theory of a basic flow is based on formulating an initial-boundary-value problem (IVP) for the linearized equation of motions (2) written in terms of the velocity component v. If the physical parameters of the flow do not vary in the direction of wave propagation, this problem can be solved by using Fourier-Laplace transform [18, 19] (see details of such a derivation in [20]) Its solution along the ray $x = x_o + Vt$, $x_o =$ constant, in the two dimensional case takes the form

$$v(y, x_0 + Vt, t) = \frac{1}{4\pi^2} \int_{\mathrm{i}\sigma-\infty}^{\mathrm{i}\sigma+\infty} \int_{-\infty}^{\infty} \frac{T(y,k,\omega+Vk)}{D(k,\omega+Vk)}\, \mathrm{e}^{\mathrm{i}(kx_0-\omega t)} \mathrm{d}k\ \mathrm{d}\omega, \tag{9}$$

where $v(y,x,t)$ is the perturbation, k is a wave number, ω is a frequency, $T(y,k,\omega)$ denotes a disturbance dependent functions, $D(k,\omega)$ is the dispersion relation function and σ is chosen bigger than $\max_{k_r}(\omega_i)$ given by the temporal stability analysis. The absolute or convective behavior of these instabilities is given by the long time asymptotic behavior of the perturbation (9) for $V = 0$. If the instability has a convective nature, the long time asymptotic behavior of (9) for various values of V will give the structure, the front velocities and the spatial amplification of wave packet.

4.1 Determination of the response to a localised disturbance

Therefore, we are interested in the long time asymptotic behavior of $v(y, x_0 + Vt, t)$ given in (9) which is the solution of the IVP along the ray $x = x_0 + Vt$ in the unstable case. The procedure is based on the analytic continuation of the inverse Fourier integral in (9)

$$R(x_0, \omega + Vk) = \int_{-\infty}^{\infty} \frac{T(y,k,\omega+Vk)}{D(k,\omega+Vk)}\, \mathrm{e}^{\mathrm{i}kx_0} \mathrm{d}k, \tag{10}$$

in the strip $\{\omega \mid 0 \leq \mathrm{Im}\,\omega \leq \sigma\}$ on the complex $\omega-$plane. If the continuation of $R(x_0, \omega + Vk)$ starting from the Bromwich contour $\{\omega \mid \mathrm{Im}\,\omega = \sigma\}$ down till and slightly below the real $\omega-$axis is possible then the solution $v(y, x_0 + Vt, t)$ decays exponentially as $t \to \infty$. On the other hand, if the analytic continuation of the function $R(x_0, \omega + Vt)$ in this strip has singular points then each of these points contributes to the growth of $v(y, x_0 + Vt, t)$.

4.2 Collision criterion

Determination of the singular points (k_0, ω_0) of $R(x_0, \omega + Vk)$ located between the Bromwich contour and the real $\omega-$axis reduces eventually to analysing the multiple $k-$roots of the dispersion relation function $D_V(k,\omega) \equiv D(k, \omega+Vk)$, for ω with $0 < \mathrm{Im}\,\omega < \sigma$, that satisfy the collision criterion as follows. In other words, when ω moves from above the Bromwich contour along the vertical line down to ω_0, which we denote by $\omega \searrow \omega_0$, the $k-$roots $k_1(\omega)$ and $k_2(\omega)$ originate in this movement on opposite sides of the real $k-$axis and collide at $k = k_0$, for $\omega = \omega_0$. This kind of a collision is called pinching of the deformed Fourier contour because the function $R(x_0, \omega + Vk)$ cannot be continued analytically in $\omega = \omega_0$ by deforming the integration contour in (10), as it is "pinched" from above and below by two $k-$roots that collide at $k = k_0$. The Fig. 3 shows examples of collisions in the complex wavenumber plane.

The dominant contribution to the asymptotics of the solution comes from the multiple $k-$roots of $D(k,\omega) = 0$ that satisfies the collision criterion and has maximum imaginary part of ω among all such roots. Then the asymptotics of the solution along the ray $x = x_o + Vt$, as $t \to \infty$, is

equal at the leading order to

$$v(y, x_0 + Vt, t) \sim C\,(y, k(V), \omega(V))\; t^S \\ \mathrm{e}^{\omega_i(V)t}\; \mathrm{e}^{-\mathrm{i}\omega_r(V)t}\; \mathrm{e}^{-k_i(V)x_0}\; \mathrm{e}^{\mathrm{i}k_r(V)x_0} \tag{11}$$

where the indices r and i denote the real and the imaginary parts, respectively. In (11), $C\,(y, k(V), \omega(V))$ is complex valued and independent of t and x_0, and $s \in \mathbb{R}$ is a rational number that depends on the number and multiplicity of the colliding $k-$roots [19]. In our case, there are two simple colliding roots and $s = -1/2$.

4.3 Saddle point method

As shown in the previous section, the function $\omega_V(k)$, satisfying $\omega_V(k_0) = \omega_0$ and $D_V(k, \omega_V(k)) \equiv 0$ in a vicinity of the collision point (k_0, ω_0) has a simple saddle point. That means that, $\mathrm{d}\omega_V(k_0)/\mathrm{d}k = 0$, $\mathrm{d}^2\omega_V(k_0)/\mathrm{d}k^2 \neq 0$, provided $\partial D_V(k,\omega)/\partial\omega \neq 0$ at (k_0, ω_0). Hence, the frequency ω as a function of k, obtained as an $\omega-$root of $D(k,\omega) = 0$ close to $(k_0, \omega_0 + Vk_0)$, satisfies $\mathrm{d}\omega/\mathrm{d}k|_{k=k_0} = V$ (or $\partial\omega_i/\partial k_r = 0$ and $\partial\omega_r/\partial k_r = V$).

In this way, we point out that the computation of collision points of k-roots of $D_V(k,\omega) = 0$ could come down to the computation of ω-roots of $D(k,\omega) = 0$ satisfying $\mathrm{d}\omega/\mathrm{d}k = V$. As the computation of the saddle points of ω-roots $D(k,\omega) = 0$ is less computer time consuming, an algorithm based on this approach has been developed and has given rather good results [21, 4, 22]. It consist to start from the saddle point (k_{mr}, ω_m) $(\omega_{mi} = \max_{k_r} \omega_i(k_r))$ given by the temporal linear analysis which is also the collision point $(k_{mr}, \omega_m - V_g k_{mr})$ of the function $D_{V_g}(k,\omega)$ with $V_g = \partial\omega_{mr}/\partial k_r$. Then, we follow the evolution of the saddle point when the ray velocity varies continuously from V_g.

The main problem of this procedure is that we have no assurance that the computed points correspond to the first collision point between the two branches of solutions of $D_V(k,\omega) = 0$ coming from the opposite sides of the real k axis as $\mathrm{Im}\omega = \sigma$. This is illustrated in Fig. 3 : in Fig. 3a, the point $k^{\blacktriangle}$ is due to collision between branches 1 and 3 and it is also obtained by the saddle point method; in Fig. 3b, the first collision point $k^{\blacktriangledown}$ comes from the branches 1 and 2; the saddle point method gives another point coming again from the collision between branches 1 and 3 but it is reached for a smaller value of ω_i.

4.4 Numerical results

Computations of the growth rate $\omega_i(V)$, the oscillatory frequency $\omega_r(V)$, the local spatial amplification rate $-k_i(V)$ and the wavenumber $k_r(V)$ across the wavepacket were performed by using the collision criterion, for various values of the Reynolds number R and for the parameters used in the experiments of Liu *et al.* [2] and the computations of Chang and Demekhin [3]. Some results are presented in Figs. 4, 5 and 6.

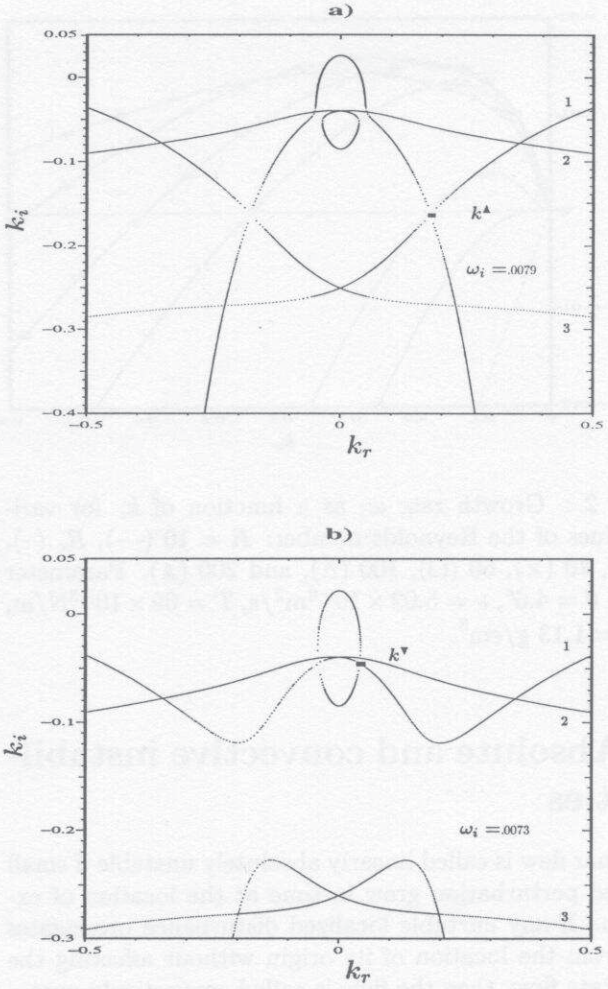

Figure 3 : Collision points in the complex wave number plane (k_r, k_i) for $R = 200, W = 14.17$ and $\theta = 4.6°$; the lines labeled $1, 2, 3$ are k-roots of $D_V(k,\omega) = 0$. The line 1 is initially in the positive k_i plane whereas the two others are in the negative part. a) V = 1.16; the collision point is due to the branches 1 and 3 for $k^{\blacktriangle} = (0.19, -0.165)$ and $\omega^{\blacktriangle} = (0.015, 0.0079)$. b) $V = 1.15$; the collision point is due to the branches 1 and 2 for $k^{\blacktriangledown} = (0.043, -0.046)$ and $\omega^{\blacktriangledown} = (0.01, 0.0073)$.

In all unstable cases considered the film flow was found to be absolutely stable as for $V < .7$ the growth rate is negative. In particular, we found that no transition from convective to absolute instability occurs for the value of the Reynolds number $R_{c/a} = R_c + (6.7\,W)^{1/3}$ predicted by the long wave analysis of Benney [23], where R_c is the critical Reynolds number given by the relation (7). For the experiments of Liu [2], $R_{c/a} \approx 23$. As already mentioned, the inadequacy of the long wave approximation for the wave packet analysis is due to the strong dispersion of waves with moderate wave lengths.

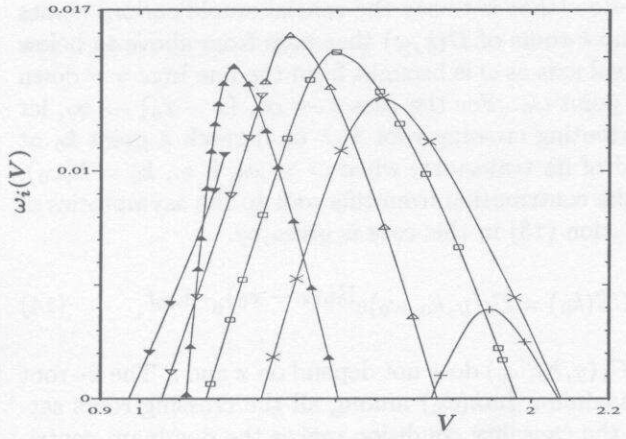

Figure 4 : growth rate $\omega_i(V)$ as functions of ray velocity V Values of the Reynolds number are $R = 20$ (+), 40 (×), 60 (□), 100 (△ and ▽), and 200 (▲ and ▼). See Fig. 2 for the other parameters values.

As shown in Fig. 4, there is only one unstable branch of $\omega_i(V)$ for each Reynolds number $R = 20$, 40, and 60 and $\theta = 4.6°$. In all these cases, the unstable branch is also recovered by using the procedure based on tracing the saddle point as described before. However, for $R = 100$, and 200, the situation in this respect is dramatically different. However the deviation of the results of the saddle point treatment from the results based on the collision criterion is more pronounced for $R = 200$ than in the case $R = 100$. For $R = 200$, the analysis based on the collision criterion produces two unstable branches of $\omega_i(V)$, marked with (▲) and (▼). The treatment based on the saddle point approach produces only one unstable branch of $\omega_i(V)$, marked in Fig. 4 with (▲). The second unstable branch, marked with (▼), is not connected by continuity in V with the saddle point corresponding to the most unstable ray. The saddle point approach gives the interval of unstable rays $(V_l^{\blacktriangle}, V_r^{\blacktriangle}) = (1.119, 1.482)$, with the length $V_r^{\blacktriangle} - V_l^{\blacktriangle} = 0.363$. The correct interval obtained using the collision criterion is $(V_l^{\blacktriangledown}, V_r^{\blacktriangle}) = (0.97, 1.482)$, its length is $V_r^{\blacktriangle} - V_l^{\blacktriangledown} = 0.512$, so it is more than 40% wider than the interval obtained with the saddle point treatment. In particular, the value of the wavenumber $k_r(\widetilde{V})$ has a jump at this point from about 0.175 on the branch (▲) to about 0.042 on the branch (▼). This means that, for V decreasing through $\widetilde{V}$, the local wavelength of the dominant part of the wavepacket $2\pi/k_r(V)$ experiences at $V = \widetilde{V}$ an abrupt increase by a factor of about 4. We expect that such a strong increase of the wavelength across the interval of ray velocities $(V_l^{\blacktriangle}, \widetilde{V}) \approx (1.115, 1.159)$ should be observable in experiments.

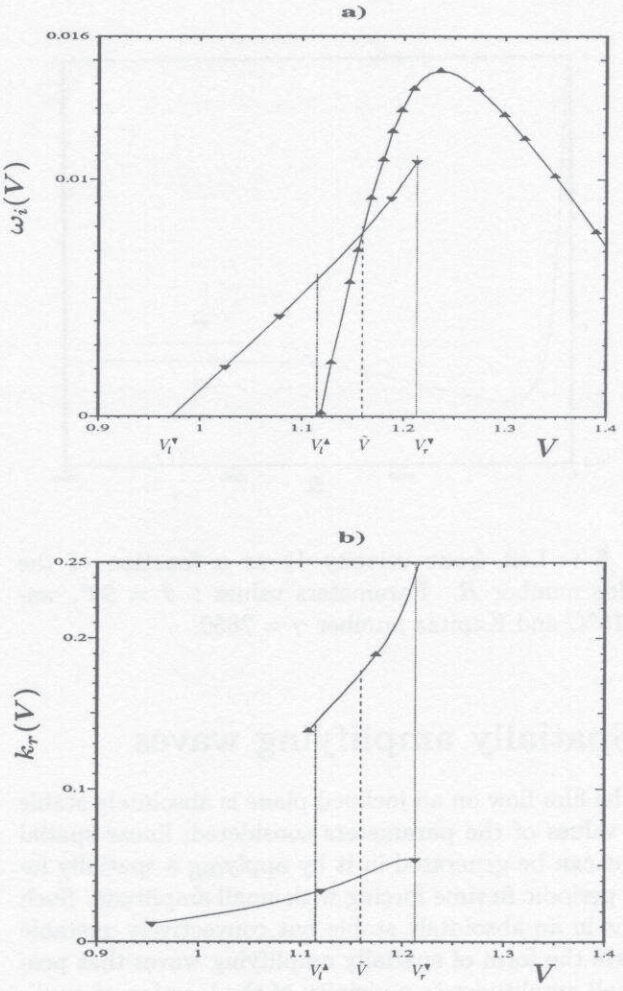

Figure 5 : Close up view of the branches marked with (▲) and (▼) in Fig. 4 near the intersection point $\widetilde{V}$.

This behavior also holds for falling films ($\theta = 90°$). In particular for parameters used by Chang and Demekhin [3] (water at 15°C), we find again that for $R > 152$, there is a bifurcation of the collision point k as the ray velocity V varies continuously. Therefore the left front velocity V_l cannot again be obtained by a saddle point method. This results is illustrated in Fig. 6 : the curve $V_l^{\blacktriangle}$ is determined thanks to the collision criterion whereas the curve $V_l^{\blacktriangledown}$ comes from the saddle point method.

The failure of the saddle point method shown by these computations casts a doubt concerning the applicability of this procedure for other flows. This remark is particularly important for 3-D flows as all numerical investigations of 3-D wave packets in fluid flows known to us were conducted until now by applying a saddle point treatment that uses the continuity argument.

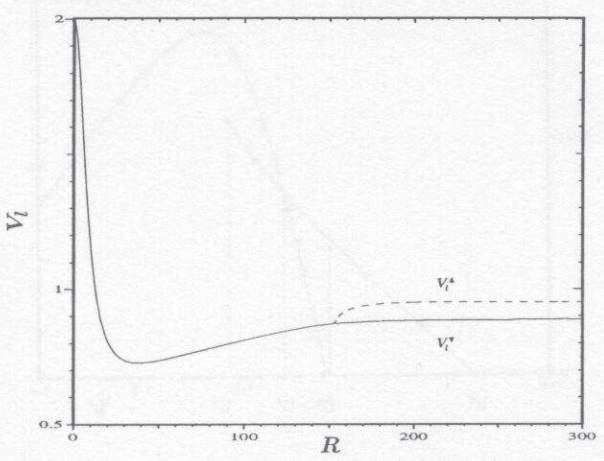

Figure 6 : Left front velocity V_l as a fonction of the Reynolds number R. Parameters values : $\theta = 90^0$, water at 15°C and Kapitza number $\gamma = 2850$.

5 Spatially amplifying waves

Since the film flow on an inclined plane is absolutely stable for all values of the parameters considered, linear spatial patterns can be generated in it by applying a spatially localised periodic in time forcing with small amplitude. Such patterns in an absolutely stable but convectively unstable flow have the form of spatially amplifying waves that possess small amplitudes in a vicinity of the location of application $x = x_0$ of the periodic forcing and amplify exponentially with the distance $|x - x_0|$ from this location in the positive or negative $(x - x_0)-$direction.

5.1 The formalism

We assume that the forcing is applied at the lower plane : the component $v(y, x, t)$ is perturbed externally on the plate $y = 1$, with all other external perturbations and the initial disturbance being zero. More general cases of external perturbations can be treated similarly. The only non-zero external perturbation is given by

$$v(1, x, t) = r(x - x_0)\mathrm{e}^{-\mathrm{i}\omega_0 t}. \tag{12}$$

Here $r(x)$ is a function with finite support, x_0 is a fixed point and ω_0 is the real frequency of the forcing. Using again Fourier-Laplace transform in order to solve the IVP, we obtain

$$v(y, x, t) = \frac{1}{4\pi^2} \int_{\mathrm{i}\sigma-\infty}^{\mathrm{i}\sigma+\infty} \frac{\mathrm{e}^{-\mathrm{i}\omega t}}{\omega - \omega_0}\mathrm{d}\omega \int_{-\infty}^{\infty} r(k)\frac{P(y,k,\omega)}{D(k,\omega)}\,\mathrm{e}^{\mathrm{i}k(x-x_0)}\mathrm{d}k. \tag{13}$$

Assumptions on the functions $r(x)$ have to be made in order to assure the convergence of the above integrals (13).

Contributions to the growing asymptotics of $v(y, x, t)$ for $x \to \infty$ (that is to say the spatial amplification) comes from the k-roots of $D(k, \omega)$ that pass from above to below the k-real axis as ω is brought from the line $\mathrm{Im}\omega = \sigma$ down to the point ω_0. For the case $t \to \infty$, $(x - x_0) \to \infty$, let a contributing crossing root $k = k(\omega)$ reach a point k_0 at the end of its trajectory, when $\omega \searrow \omega_0$, i. e., $k_0 = k(\omega_0)$. Then the contribution from this root to the asymptotics of the solution (13) in this case is given by

$$CS(k_0) = C_1(y, k_0, \omega_0)\mathrm{e}^{\mathrm{i}k_0(x-x_0)}\mathrm{e}^{-\mathrm{i}\omega_0 t}, \tag{14}$$

where $C_1(y, k_0, \omega_0)$ does not depend on x and t. The $k-$root with maximum $\mathrm{Im}k(\omega_0)$ among all the crossing roots satisfying the causality condition makes the dominant contribution to the asymptotics, for $t \to \infty$, $(x - x_0) \to \infty$.

5.2 Numerical results

For all supercritical Reynolds numbers there are spatially amplifying waves that amplify in the positive $x-$direction, i. e., when $(x - x_0) \to \infty$. Depending on the Reynolds number R and the angle θ there are amplifying waves of the shear mode or of both the shear and the surface modes. For the angle $\theta = 4.6^0$ used in the computations the minimum critical Reynolds number of the shear mode over all T is well above 1000 [14], i. e., well above the maximum Reynolds number $R = 200$. Hence, spatially amplifying waves of only the surface mode are present.

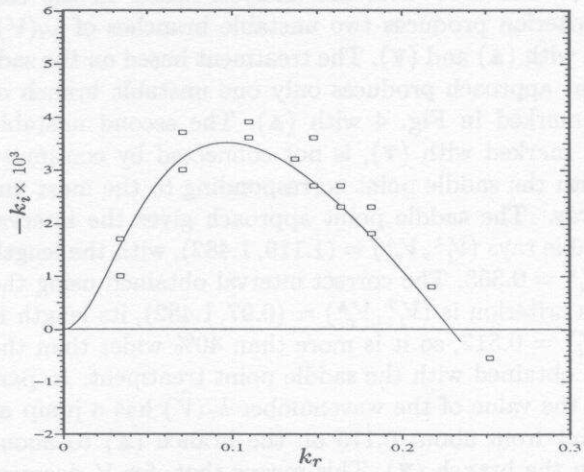

Figure 7 : Spatial growth rate $-k_i$ as functions of wavenumber k_r. Measurements (□) are taken from Fig. 14 in [2]. The parameter values are $\theta = 4.6^0$, $\nu = 4.89 \times 10^{-6}\mathrm{m}^2/\mathrm{s}$, $T = 69 \times 10^{-3}\mathrm{N/m}$ and $\rho = 1.13\ \mathrm{g/cm}^3$.

Formally, this computation corresponds to solving spatial stability problem and consist of finding k-roots of $D(k,\omega) = 0$ for $\omega = \omega_r$. In terms of the expression (14), ω_r corresponds to ω_0, and $k_r + ik_i$ is k_0. For the case when the temporal and the spatial growth rates are small, the following transformation relating approximately these growth rates was proposed by Gaster [5]

$$-k_i(S) = \omega_i(T)/\frac{\partial \omega_r}{\partial k_r}, \tag{15}$$

where S and T mean that the values are obtained in the spatial and the temporal stability analyses, respectively. The Gaster transformation is widely utilised for computing spatial growth rates of normal modes by using computed temporal growth rates. This saves greatly the computation time because spatial stability computations are considerably more time consuming than temporal stability ones. In [24], a mathematical example was presented in which all the premises of the Gaster [5] analysis were fulfilled but the formula (15) gave incorrect results indicating that the Gaster transformation should be used with caution. Since in the present analysis we performed both the temporal and the spatial stability computations, we used the opportunity of checking the applicability of the Gaster formula (15). The outcome of this check is quite interesting. It comes out that the formula (15) not only gives good approximation for the spatial growth rate when the growth rates are very small, but moreover, the dependence of the spatial growth rate given by (15) on the real part of frequency ω_r is practically indistinguishable from the results obtained in the direct spatial stability computations, for the entire range of unstable frequencies. In the present case, the Gaster transformation allows us to get the spatial amplification in the entire domain of unstable k_r as $\omega_r(T)$ given by the temporal stability analysis is almost a linear function of k_r.

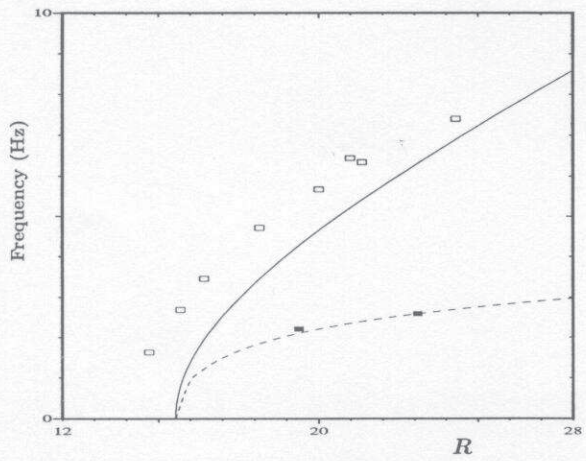

Figure 8 : cutoff frequency (–) and most rapidly amplified frequency (- -) as functions of the Reynolds number R for $\theta = 4.6°$. Experimental data (□) and (■) are taken from Fig. 18 in [2]. See Fig. 2 for the other parameters values.

Our computations are in fairly good agreement with the experimental results of Liu *et al.* [2]. In Fig. 7, we compare the computed growth rate with the measurements for $\theta = 4.6°$, $R = 23$ and $W = 62$, and it is in good agreement with the experiments. In particular, the most unstable wave number and the cutoff wave number are correctly predicted.

The computations and the measurements of the cutoff and the most rapidly amplified frequencies are plotted in Fig. 8. Although there is a discrepancy between the cutoff frequencies, the shape delineated by the measurement points parallels the shape of the computed curve. The most rapidly amplified frequencies compare well.

Nomenclature

g	=	gravitational acceleration, N/s^2
k	=	complex wave number
k_r	=	real part of wave number
k_i	=	spatial growth
R	=	Reynolds number
T	=	surface tension, N/m
U	=	parabolic profile, m/s
U_0	=	surface velocity, m/s
V	=	ray velocity
V_l	=	left front velocity
W	=	Weber number

Greek Letters

θ	=	angle, degree
μ	=	viscosity, $N.s/m^2$
ν	=	kinematic viscosity, m^2/s
ρ	=	density, g/cm^3
ω	=	complex pulsation
ω_r	=	real part of the pulsation
ω_i	=	growth rate

References

[1] R.J. BRIGGS. *Electron-Stream interaction with Plasmas.* MIT press, Cambridge, 1964.

[2] J. LIU, J.D. PAUL, and J.P. GOLLUB. Measurements of the primary instabilities of film flows. *J. Fluid Mech.*, 250:69–101, 1993.

[3] H.-C. CHANG and E.A. DEMEKHIN. Solitary wave formation and dynamics on falling film. *Advances in Applied Mechanics*, 32:1–58, 1996.

[4] R.J. DEISSLER. The convective nature of instability in plane Poiseuille flow. *Phys. Fluids*, 30:2303–2305, 1987.

[5] M. GASTER. A note on the relation between temporally-increasing and spatially-increasing disturbances in hydrodynamic stability. *J. Fluid Mech.*, 14:222–224, 1962.

[6] J. LIU and J.P. GOLLUB. Onset of spatially chaotic waves on flowing films. *Phys. Review Letters*, 70:2289–2292, 1993.

[7] J. LIU and J.P. GOLLUB. Solitary wave dynamics of film flows. *Phys. Fluids*, 6:1702–1712, 1994.

[8] T.B. BENJAMIN. Wave formation in laminar flow down an inclined plane. *J. Fluid Mech.*, 2:554–574, 1957.

[9] C.-S. YIH. Stability of parallel laminar flow with a free surface. In *Proc. 2nd US congr. on Applied Mechanics*, pages 623–628, AMSE, 1955.

[10] J. LIU, J.B. SCHNEIDER, and J.P. GOLLUB. Three-dimensional instabilities of film flows. *Phys. Fluids*, 7(1):55–67, 1995.

[11] H.-C. CHANG. Wave evolution on fallling film. *Ann. Rev. Fluid Mech.*, 26:103–136, 1994.

[12] Y.L. JOO and S.H. DAVIS. Instabilities of three-dimensional viscous falling films. *J. Fluid Mech.*, 242:529–547, 1992.

[13] S.P. LIN. Finite amplitude side-band stability of a viscous film. *J. Fluid Mech.*, 63:417–429, 1974.

[14] J.M. FLORYAN, S.H. DAVIS, and R.E. KELLY. Instabilities of a liquid film flowing down a slightly inclined plane. *Phys. Fluids*, 30:983–989, 1987.

[15] S. ORSZAG. Accurate solution of the Orr-Sommerfeld equation. *J. Fluid Mech.*, 50(4):689–703, 1971.

[16] A. BERS. Theory of absolute and convective instabilities. In F. Cap G. Auer, editor, *International Congress on Waves and Instabilities in Plasmas*, pages B1–B52, 1973.

[17] P. HUERRE and A. MONKEWITZ. Local and global instabilities in spatially developing flows. *annu. Rev. Fluid Mech.*, 22:473–537, 1990.

[18] P. HUERRE and P.A. MONKEWITZ. Absolute and convective instabilities in free shear layers. *J. Fluid Mech.*, 159:151–168, 1985.

[19] L. BREVDO. A study of absolute and convective instabilities with an application to the eady model. *Geophys. Astrophys. Fluid Dyn.*, 40:1–92, 1988.

[20] L. BREVDO, P. LAURE, F. DIAS, and T.J. BRIDGES. Linear pulse ans signalling in a film flow on an inclined plane. *J.Fluid Mech.*, 1998. in preparation.

[21] A.J. SIMMONS and B.J. HOSKINS. The downstream and upstream development of unstable baroclinic waves. *J. Atmos. Sci.*, 36:1239–1254, 1979.

[22] L. BREVDO. Convectively unstable wave packets in the Blasius boundary layer. *Z. Angew. Math. Mech.*, 75(6):423–436, 1995.

[23] D.J. BENNEY. Long waves on liquid films. *J. Math. Phys.*, 45:150–155, 1966.

[24] L. BREVDO. A note on the Gaster transformation. *Z. Angew. Math. Mech.*, 72(7):305–306, 1992.